Optical Anisotropy as a Probe of Structural Order by Stokes Polarimetry

Dennis K. Hore and Almeria L. Natansohn

Department of Chemistry, Queen's University, Kingston ON, K7L 3N6, Canada

Paul L. Rochon*

Department of Physics, Royal Military College, P.O. Box 17000, Station Forces, Kingston ON, K7L 7B4, Canada

Received: April 1, 2002; In Final Form: July 3, 2002

Structural order often manifests itself in the anisotropic optical phenomena birefringence and dichroism. Such properties of a material cause changes in the polarization of a probe beam. Characterization of the optical anisotropy, and subsequent inference on the structural arrangement of molecules responsible, may be accomplished in two stages. First, Stokes polarimetry is used to determine the polarization change in the transmitted light. Next, a model of the polarization transfer is used to fit the data in order to obtain values of the birefringence and dichroism which may serve as quantitative order parameters. The technique may be applied to linear as well as circular anisotropy, but is perhaps most valuable for cases in which both types coexist and therefore need to be separated. Our polarimeter is simple in construction and may be assembled from common optical elements.

1. Introduction

In many cases it is useful and interesting to know how molecules are arranged in a solid, either as a result of rearrangement due to an external stimulus, self-assembly, or in their natural state. Polarized light serves as an excellent probe of molecular order because it is (in most cases) noninvasive and may "query" the sample in its natural form, often without any preparation.

For some time now, our group has been interested in the characterization of molecular ordering which may be photoinduced in thin films of polymers containing photoresponsive azobenzene groups.[1,2] Most of our studies and most of the studies in the literature have focused on the attainment of uniaxial order from a previously amorphous state prior to irradiation. The axis of orientation is determined by the azimuth of a linearly-polarized pump beam.[3,4] In the case of liquid-crystalline polymers where the materials are initially ordered into uniaxial clusters or domains, it is possible to change the existing axes of orientation in response to the polarization of the pump.

More recently, there has been interest in studying the type of ordering that is induced in these materials upon irradiation with circularly polarized light.[5−9] Our observations for such experiments include the induction of both linear and circular anisotropy, and so we required an experimental method and subsequent treatment of the data that provided a clear separation of these types of ordering. In achieving this, we realized that this approach also provided a refinement of the characterization of uniaxial linear anistropy which may, under some circumstances, provide additional information on the ordering.

Stokes polarimetry, also referred to as transmission ellipsometry, is a popular choice for the determination of optical anisotropy[7,10] because it provides a complete description of the polarization of the transmitted light by providing both its azimuth and ellipticity. The primary benefit of Stokes polarimetry is indeed the separation of linear and circular anisotropy. (Noteworthy here is that linear and circular anisotropy both change the azimuth and ellipticity of the input beam. In cases where they are present in tandem, their separation may be achieved based on the dependence of the optical constants on the incident polarization azimuth, as will be seen in section 3.3.) It does, however, offer an advantage in the determination of linear anisotropy alone over less sophisticated techniques, such as birefringence determination through crossed polarizers or dichroism measurement with a single polarizer. It is often desirable to probe the sample outside of its absorption band, especially in the case of photoinduced orientation where the probe should not reorient the sample. Here the birefringence provides a more useful order parameter because the refractive index does not decay as rapidly as does the absorption coefficient when moving away from the absorbance maximum. The presence of a nonnegligible dichroism, however, does not allow accurate measurement of the birefringence by simple means because the dichroism contributes to the signal through the crossed polarizers.

Recently there have been accounts of instruments which, for example, allow the determination of very small optical rotation,[11] work in real-time,[12] raster the sample surface to produce a 2D image,[13,14] or operate over a range of wavelengths in a spectroscopic fashion.[15−18] While our instrument does not have any of these advanced capabilities, it is simple in design and construction and affords the material's optical constants with a minimum amount of data treatment.

In the first part of this paper we outline the Stokes polarimetry experiment, including details on our polarimeter configuration. Next, the data analysis that provides the values of the optical

* Corresponding author. Phone: 613-541-6000 ext 6451. Fax: 613-541-6040. E-mail: rochon-p@rmc.ca

10.1021/jp025877u CCC: $22.00
Published on Web 08/14/2002

constants is illustrated in three case studies. First, the linear anisotropy, which is photoinduced in an amorphous polymer blend, is presented in detail, showing the steps that are involved in determining the birefringence, dichroism, and orientation of the optical axis from the raw data. Second, the concentration of a sucrose solution is determined as a demonstration of circular anisotropy. Finally, an example is presented in which linear and circular anistropy have been simultaneously photoinduced in a liquid-crystalline polymer, and all five order parameters are determined.

1.1. Qualitative Description of Optical Anisotropy which Results from Structural Order. Linear anistropy, in a structural sense, often exists as a case of uniaxial alignment. This may be an intrinsic state of the material such as a crystalline solid or liquid crystal, but it may also be induced by rubbing, stretching, irradiating, or applying an external electric or magnetic field. In all of these cases, an optical axis exists or develops and the refractive index and absorption coefficient of the material show a directional dependence. If linearly polarized light impinges upon a uniaxial arrangement of molecules with an arbitrary orientation, the component of the optical field parallel to the absorbing axis of the molecules will be attenuated to a greater extent than the component perpendicular to this axis. This phenomenon is referred to as linear dichroism, $\Delta\alpha_{lin} \equiv \alpha_y - \alpha_x$, where α is the absorption coefficient and x and y are in the laboratory frame of reference. The component that is absorbed preferentially is also retarded with respect to the other, and a phase shift develops. This is the origin of the linear birefringence, $\Delta n_{lin} \equiv n_y - n_x$, where n is the real part of the complex refractive index. As a result of these two related interactions, the azimuth and ellipticity of the probe beam change while traversing the sample, and may be measured in the transmission.

Circular anisotropy may exist at the structural level of a single molecule in the case of a chiral center. A collection of such molecules, a sugar solution for example, will exhibit circular optical anisotropy. Here it is the handedness of the molecules, and not their arrangement with respect to one another, that is responsible for the phenomenon. A second example, on a supramolecular scale, is a helix which may be assembled in a manner that is either right- or left-handed. When such a structure encounters light, a similar optical anisotropy is observed as in the case of a chiral solution. To qualitatively describe the effect of this anisotropy on the probe beam, it is convenient to picture incident linearly-polarized light to be a superposition of left- and right-circularly polarized states. When this beam passes through a helix or a solution of chiral molecules, one of the *circular* polarization states is preferentially absorbed. This is circular dichroism, $\Delta\alpha_{cir} \equiv \alpha_L - \alpha_R$, and it has the effect of making the output beam elliptically polarized without changing its azimuth. As a result of this dichroism, however, the component that is absorbed to a greater extent is also retarded, resulting in a phase shift in the circular components. This is circular birefringence, $\Delta n_{cir} \equiv n_L - n_R$, also commonly referred to as optical activity or optical rotation. From the standpoint the linearly-polarized probe beam, it appears that the azimuth has been rotated.

2. Stokes Polarimetry

In a Stokes polarimetry experiment, light of a known polarization is incident on a sample and the polarization of the transmitted light is determined. Here linearly polarized light is used as a probe and, in the most general case, the light that emerges from the sample is elliptically polarized. The polarization ellipse will be characterized by determining its Stokes vector, defined by

$$S = \begin{bmatrix} S_0 \\ S_1 \\ S_2 \\ S_3 \end{bmatrix} = \begin{bmatrix} I_{total} \\ I_0 - I_{90} \\ I_{45} - I_{-45} \\ I_{rcp} - I_{lcp} \end{bmatrix} = \begin{bmatrix} E_x E_x^* + E_y E_y^* \\ E_x E_x^* + E_y E_y^* \\ E_x E_y^* + E_y E_x^* \\ i(E_x E_x^* + E_y E_y^*) \end{bmatrix} \quad (1)$$

The Stokes vector is a convenient choice for this description because all of the S_j represent intensities and so are readily determined in the lab. S_0 is the total intensity; S_1 is the intensity difference between horizontally and vertically polarized components; S_2 is the difference in intensity between components polarized at $+45°$ and $-45°$; S_3 is the difference between right- and left-circularly polarized light intensities.

Our polarimeter (Figure 1) consists of a HeNe laser (λ = 632.8 nm) whose polarization direction is varied by means of a Glan-Thompson prism. (Since the laser produces linearly polarized light, it is first made circular using a quarter waveplate before it is incident on the GT prism.) This linearly polarized light with variable azimuth impinges on the sample at normal incidence and then reaches a rotating quarter-wave plate[19] (ω = 20 Hz). Finally, the beam passes through a horizontal polarizer before reaching the detector. Our setup may therefore be considered as an ellipsometer in the PSCA (polarizer-sample-compensator-analyzer) configuration. A reference frequency twice that of the rotating waveplate (2ω = 40 Hz) is used for the detection of the fundamental; then 4ω may be readily detected as the second harmonic of the reference.

It is convenient to use a Müller calculus formalism to describe the experimental setup[20,21] although a Jones calculus is also a popular choice.[22] The beam emerging from the sample, whose polarization state we wish to analyze, is represented by the Stokes vector

$$S = \begin{bmatrix} S_0 \\ S_1 \\ S_2 \\ S_3 \end{bmatrix}, \quad (2)$$

the rotating waveplate with $\theta = 2\omega t$ has the Müller matrix

$$W = \begin{bmatrix} 1 & 0 & 0 & 0 \\ 0 & \cos^2\theta & \sin\theta\cos\theta & -\sin\theta \\ 0 & \sin\theta\cos\theta & \sin^2\theta & \cos\theta \\ 0 & \sin\theta & -\cos\theta & 0 \end{bmatrix} \quad (3)$$

and the horizontal analyzer is described by

$$P = \begin{bmatrix} 1/2 & 1/2 & 0 & 0 \\ 1/2 & 1/2 & 0 & 0 \\ 0 & 0 & 0 & 0 \\ 0 & 0 & 0 & 0 \end{bmatrix} \quad (4)$$

The light reaching the detector is given by the matrix product $S' = PWS$. The intensity comes from the first element of S', which is

$$I(\theta) = \frac{1}{2}S_0 + \frac{1}{2}S_1\cos^2\theta + \frac{1}{2}S_2\sin\theta\cos\theta - \frac{1}{2}S_3\sin\theta \quad (5)$$

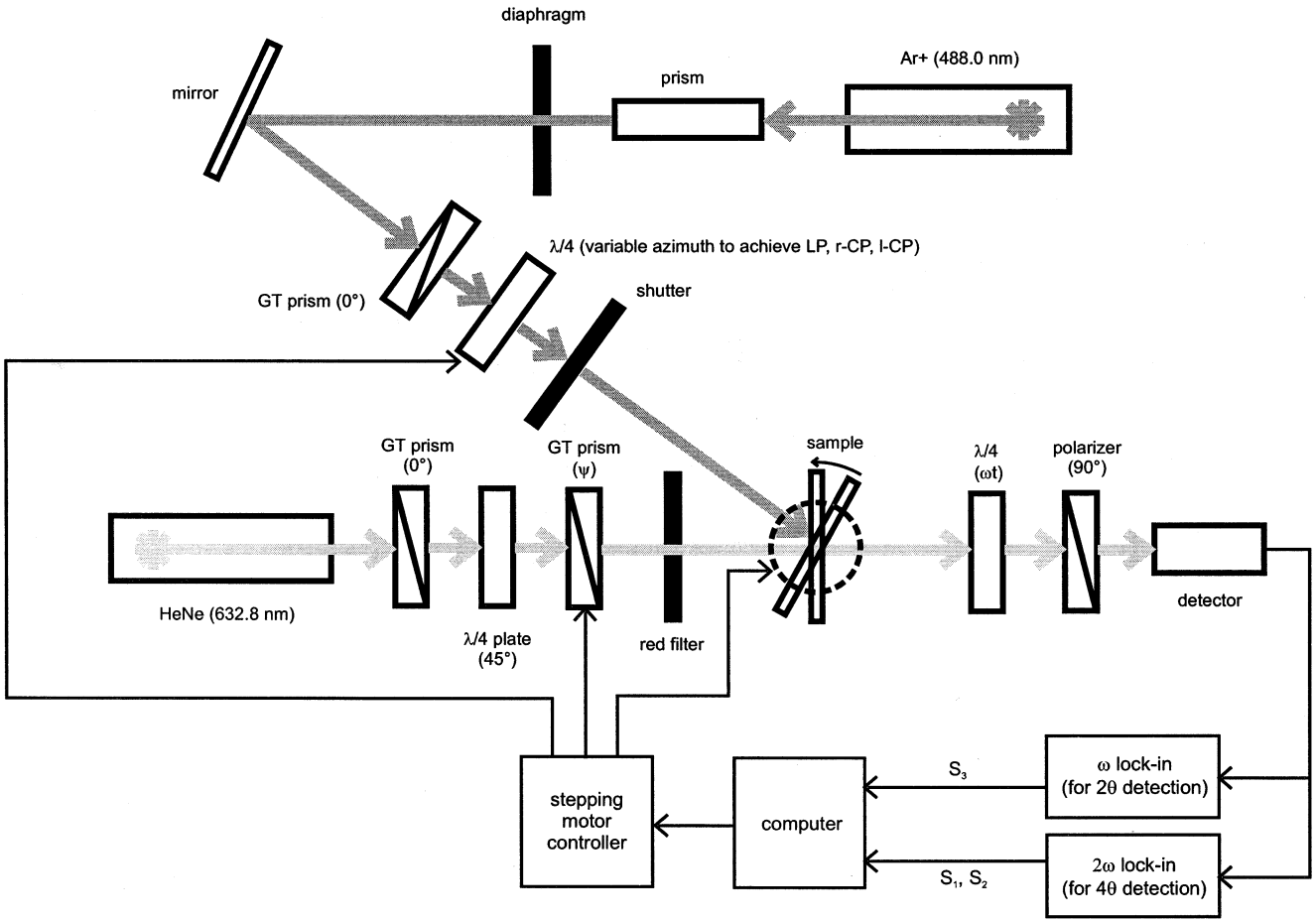

Figure 1. Optical bench for Stokes polarimetry of photoinduced orientation. The sample may be rotated about the *y*-axis so that irradiation and measurement are both at normal incidence.

Rearranging this using common trig identities results in[21]

$$I(\theta) = \frac{1}{2}\left(S_0 + \frac{1}{2}S_1\right) + \frac{1}{4}S_1 \cos 2\theta + \frac{1}{2}S_2 \sin 2\theta - \frac{1}{2}S_3 \sin \theta \quad (6)$$

From the form of eq 6 it is easily identifiable that S_3 is obtained from the signal at the fundamental (actually the second harmonic of the rotation frequency of the waveplate), and S_1 and S_2 come from the quadrature and in-phase components of the second (fourth) harmonic. Rotating the waveplate continuously thus allows the Fourier analysis to be done by two lock-in amplifiers, rather than in the data treatment as is traditionally the case.[23] S_0 is contained in the DC component of the signal but is more easily obtained from

$$S_0 = \sqrt{S_1^2 + S_2^2 + S_3^2} \quad (7)$$

if no depolarization has occurred upon traversing the sample. Finally, the Stokes parameters are normalized by dividing by the light intensity incident on the sample, $I_0(\psi)$, for every value of the incident polarization angle. The initial phase was adjusted by placing all of the signal in the quadrature component of the second harmonic for $\psi = 0$ before mounting the sample, since we know that $S_1(0) = 1$ for an isotropic sample (air). Representative data collected during an experiment are shown in Figure 2.

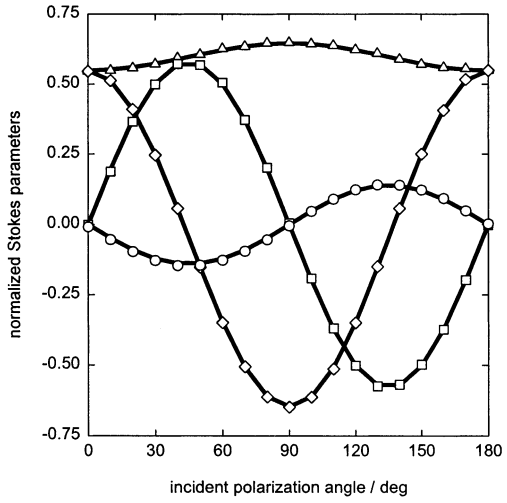

Figure 2. Representative data showing the Stokes parameters as the incident polarization angle is varied from $0 \leq \alpha \leq \pi$ with $\triangle$ S_0, $\diamond$ S_1, $\square$ S_2, and $\bigcirc$ S_3. The solid lines show the fit obtained for $\Delta n_{lin} = (-4.99 \pm 0.25) \times 10^{-3}$, $\Delta\alpha_{lin} = (-1.47 \pm 0.08) \times 10^{-2}$ nm^{-1}, $\theta = (-0.0131 \pm 0.0006)°$.

3. Case Studies

Having determined the Stokes parameters, and therefore the polarization of the transmitted light, the last step is to model the polarization transfer by the sample so that the experimentally determined polarization state may be attributed to numerical values of the birefringence and dichroism. This will be shown first for the case of linear anisotropy, followed by an example of circular anisotropy, and then a situation where both types of ordering are present and need to be separated.

In addition to tracking changes in field amplitude and phase during propagation in birefringent and dichroic media, there are

two small but important considerations that are included in our models. First, the Fresnel coefficients which account for reflection and transmission at the sample surfaces are anisotropic. Neglect of this anisotropy may cause changes in transmittance (due to anisotropic reflection) to be interpreted as dichroism, for example. Second, the materials of interest to us are thin films, so the effects of thin-film interference should not be ignored. We need to model the propagation of the field through the sample as accurately as possible in order to account for the polarization of the transmitted light, upon which we base all our conclusions as to the molecular arrangement.

3.1. Linear Anisotropy. *3.1.1. Description of the Polarization Change.* The influence of the optical constants on the polarization state of a probe beam is readily modeled using a Jones calculus approach. The incident light is described by the Jones vector

$$E_{\text{in}} = \begin{bmatrix} \cos\psi \\ \sin\psi \end{bmatrix} \tag{8}$$

for linearly polarized light that makes an angle ψ with the positive x-axis. The goal is to construct a polarization transfer function, T, so that

$$E_{\text{out}} = \frac{TE_{\text{in}}}{t_{\text{ag}}} \tag{9}$$

provides a description of the output field and therefore the transmitted light. (The factor t_{ag}, which appears in the denominator, is the Fresnel coefficient for a single air-glass interface, required because the experimental data is normalized with a baseline obtained with only the glass substrate.) The transfer function for linear birefringence and dichroism is obtained by considering the problem of interference from two surfaces, as illustrated in Figure 3. It is required that the components of the electric and magnetic fields tangential to each interface be continuous across the interfaces. At the air-film interface this results in

$$E^+_{\text{air}} + E^-_{\text{air}} = E^+_{\text{film}} + E^-_{\text{film}} \tag{10}$$

$$H^+_{\text{air}} + H^-_{\text{air}} = H^+_{\text{film}} + H^-_{\text{film}} \tag{11}$$

where the superscripts indicate whether the propagation is along the $+z$ direction or the $-z$ direction. Making use of the relation

$$\vec{H} = \frac{\epsilon_0}{\mu_0} n \hat{k}_0 \times \vec{E} \tag{12}$$

where $k_0 \equiv 2\pi/\lambda$ is the wavevector, eq 11 may be written as

$$\sqrt{\frac{\epsilon_0}{\mu_0}} n_{\text{air}} (E^+_{\text{air}} - E^-_{\text{air}}) = \sqrt{\frac{\epsilon_0}{\mu_0}} n_{\text{film}} (E^+_{\text{film}} - E^-_{\text{film}}) \tag{13}$$

A similar set of expressions may be written for the film-glass interface. The fields $E^+_{\text{film}}{}'$, $E^-_{\text{film}}{}'$, $H^+_{\text{film}}{}'$, and $H^-_{\text{film}}{}'$ at the back interface shown in Figure 3 may be related to the corresponding fields at the front interface by considering the extra phase accumulated as a result of travelling inside the material. For example,

$$E^+_{\text{film}}{}' = E^+_{\text{film}} \mathrm{e}^{\mathrm{i}k_0 n_{\text{film}} d} \tag{14}$$

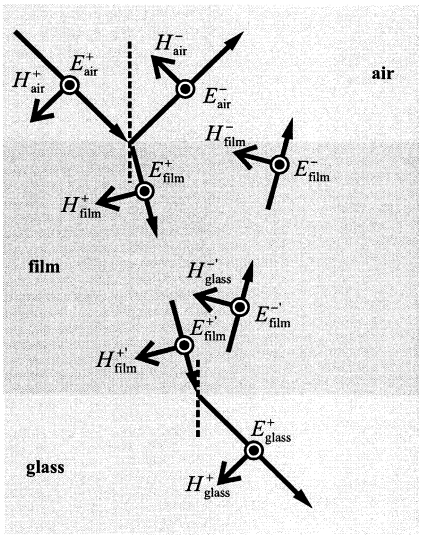

Figure 3. Transmission functions for interference from two surfaces derived from a consideration of the continuity of the tangential components of E and H at each surface. Inside an anisotropic film, E_{film} is replaced with $E^{\text{slow}}_{\text{film}}$ and $E^{\text{fast}}_{\text{film}}$ for the appropriate axes; the same applies to H, n, and κ. For our experients, only normal incidence is considered; the wavevectors are depicted in oblique incidence so that the incident and reflected waves may be described clearly.

where d is the sample thickness. Making these substitutions and again applying eq 12 gives, for the film-glass boundary,

$$E^+_{\text{film}} e^{\mathrm{i}k_0 n_{\text{film}} d} + E^-_{\text{film}} \mathrm{e}^{-\mathrm{i}k_0 n_{\text{film}} d} = E^+_{\text{glass}} \tag{15}$$

$$\sqrt{\frac{\epsilon_0}{\mu_0}} n_{\text{film}} (E^+_{\text{film}} \mathrm{e}^{\mathrm{i}k_0 n_{\text{film}} d} - E^-_{\text{film}} \mathrm{e}^{-\mathrm{i}k_0 n_{\text{film}} d}) = \sqrt{\frac{\epsilon_0}{\mu_0}} n_{\text{glass}} E^+_{\text{glass}} \tag{16}$$

These equations may be used to solve for the desired transmission coefficient $t = E^+_{\text{glass}}/E^+_{\text{air}}$. For simplicity, the above treatment has considered the film to be isotropic. Really, we want to solve this problem twice; once for each eigenpolarization. To achieve this we simply replace n_{film} with $n_{\text{slow}} \equiv n^{\text{film}}_{\text{slow}} + i\kappa^{\text{film}}_{\text{slow}}$ and $n_{\text{fast}} \equiv n^{\text{film}}_{\text{fast}} + i\kappa^{\text{film}}_{\text{fast}}$ where $n_{\text{slow}} = n_{\text{iso}} - {}^1/_2\Delta n_{\text{lin}}$, in keeping with the sign convention $\Delta n_{\text{lin}} \equiv n_y - n_x$, and the slow axis (high index) is along x. Here the attenuation of the field is a result of dichroism as described by κ, the complex part of the refractive index. This is related to the absorption coefficent α by

$$\begin{aligned} A = \alpha d \Rightarrow \alpha &= \frac{A}{d} \\ &= -\frac{1}{d}\log\left(\frac{I}{I_0}\right) \\ &= -\frac{1}{d}\log[\mathrm{e}^{ik(n+i\kappa)d}\mathrm{e}^{-ik(n-i\kappa)d}] \\ &= \frac{2k\kappa}{\ln 10} \approx \frac{5.458}{\lambda}\kappa \end{aligned} \tag{17}$$

where A is the absorbance and I and I_0 are the intensities of the transmitted and incident light, respectively. Now we have

$$t_{\text{slow}} = 2n_{\text{air}} \Big/ \left[(n_{\text{air}} + n_{\text{glass}}) \cos(k_0 n_{\text{slow}} d) - i\left(\frac{n_{\text{air}} n_{\text{glass}}}{n_{\text{slow}}} + n_{\text{slow}}\right) \sin(k_0 n_{\text{slow}} d) \right] \tag{18}$$

and an exactly analogous expression for t_{fast}.

Before descending on the sample at the air-film interface, the incident light is transformed from an *xy* basis to a fast-slow basis by means of the rotation operator $R(\theta)$ so that linear components of the electric field propagate along the optical axes of the sample. The final polarization transfer matrix is then obtained with

$$T = R(-\theta)\begin{bmatrix} t_{slow} & 0 \\ 0 & t_{fast} \end{bmatrix} R(\theta) \qquad (19)$$

3.1.2. Obtaining the Optical Constants. Values of Δn_{lin}, $\Delta\alpha_{lin}$, and θ in eq 19 which best fit the experimental data to eq 9 are obtained with a three-dimensional exhaustive search algorithm. A parameter space is initially constructed that is certain to contain the best fit values. Each tuple (Δn_{lin}, $\Delta\alpha_{lin}$, θ) that occupies the volume is considered in turn, and the fitting error (E) is evaluated as the sum of the least-squares residuals.

$$E = \sum_{j=0}^{3}\sum_{k=1}^{N} (f(\Delta n_{lin}, \Delta\alpha_{lin}, \theta; \psi_k) - S_{j,k})^2 \qquad (20)$$

This error function was chosen because it gives more weight to further outliers than does a linear residual, for example. Once the volume element corresponding to the best-fit tuple (smallest E) has been identified, a new parameter space is constructed having boundaries that are the neighbors of the volume element in the previous space. This process continues until a convergence criterion has been satisfied along each dimension. Once one of the parameters converges, the parameter space is reduced to a $(N - 1)$-dimensional volume to hasten the fitting process.

So the optical characterization of an anisotropic sample proceeds according to the following scheme. (1) Measure $S_j(\psi)$, the components of the Stokes vector for each incident polarization angle. (2) Make initial guesses for values of the anisotropic material constants that appear in the model (in this case Δn_{lin}, $\Delta\alpha_{lin}$, and the orientation of the optical axis, θ). (3) Using these values, construct the explicit polarization transfer function, T, from eq 19. (4) Use T to arrive at the components of the transmitted light using eq 9. (5) From E_{out} use eq 1 to determine the corresponding S_j. (6) Compare these calculated S_j with those obtained experimentally in step 1. Vary the values of the material constants in step 2 to obtain a better approximation to T.

Steps 4−6 are repeated until convergence criteria have been satisfied. The "best fit" values of the anisotropic material constants have then been determined.

3.1.3. Results. A 4.8-μm film of the amorphous polymer blend p(DR1M-*blend*-MMA)[24] was prepared by spin casting a mixture of 11% wt/wt pDR1M[25] and poly(methyl methacrylate) in a tetrahydrofuran solution. (Structures of the repeat units for these polymers are shown in Figure 4a.) The film was then heated to 140 °C (about 10−20 °C above the glass transition temperature) in order to remove any anisotropy which may have been caused by the spinning. Measurement of the Brewster angle yielded a refractive index of 1.50. The film was irradiated in short intervals for a total of 20 min with vertically polarized light from a 488-nm Ar^+ laser (I = 8 mW/cm^2). After each irradiation period, the sample was allowed to relax for 5 min before $S_j(\psi)$ were measured with the polarimeter. We have determined that reorientation of the chromophores after the pump is switched off is very small (less than 5% loss in linear birefringence) and is complete after about 1 min. Results of the data analysis are shown in Figure 5. Initially there is a very small amount of

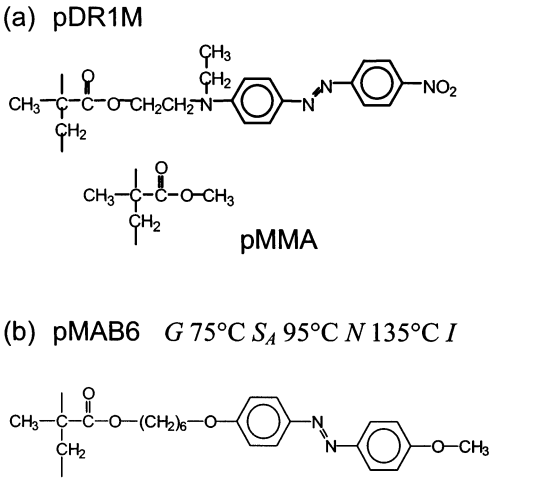

Figure 4. Chemical structures for the repeat units of (a) the amorphous polymers pDR1M and pMMA which are contained in the blend and (b) the liquid-crystalline polymer pMAB6.

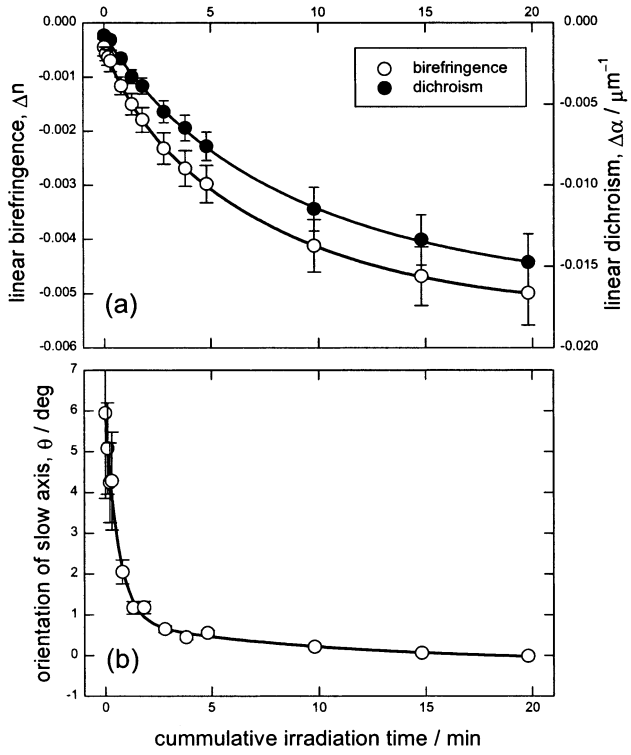

Figure 5. Evolution of (a) birefringence, dichroism, and (c) orientation of the optical axis during irradiation of a 4.8-μm sample of p(DR1M-*blend*-MMA) with vertically polarized Ar^+ light, λ = 488 nm, I = 8 mW/cm^2.

anisotropy present ($|\Delta n_{lin}|$, $|\Delta\alpha_{lin}| < 0.001$) and the near-random arrangement of the chromophores resulted in an average optical axis oriented 6° from the horizontal. As the sample is irradiated, Δn_{lin} and $\Delta\alpha_{lin}$ become increasingly negative, indicating that the refractive index along the horizontal direction is becoming increasingly greater than that along the vertical direction. Also, the molecular axis in the irradiated area quickly tends toward the horizontal. This is the well-known photoinduced reorientation of the azobenzene-containing groups in the DR1M side chain.[3,4] These groups undergo repeated trans−cis−trans isomerization cycles, thereby randomly changing their position, until they happen to fall perpendicular to the polarization direction of the pump laser. In this position, they can no longer absorb the light and so the isomerization cycles and subsequent reorientations cease. It is by this mechanism that the azo groups

end up oriented horizontally, giving the material a higher refractive index and absorption coefficient along this direction.

3.2. Circular Anisotropy. *3.2.1. Description of the Polarization Change.* The treatment of circular anisotropy is in some sense more simple than the case of linear anisotropy since the refractive indices and absorption coefficients here (and the corresponding anisotropies Δn_{cir} and $\Delta\alpha_{cir}$) are for the circularly polarized eigenstates. As a result, the Fresnel coefficients that govern transmission through the interfaces are isotropic.

For the anisotropic contribution to the polarization transfer, we start with the transfer functions for birefringence

$$T_{CB} = \begin{bmatrix} \cos\left(\frac{1}{2}k_0\Delta n_{cir}d\right) & \sin\left(\frac{1}{2}k_0\Delta n_{cir}d\right) \\ -\sin\left(\frac{1}{2}k_0\Delta n_{cir}d\right) & \cos\left(\frac{1}{2}k_0\Delta n_{cir}d\right) \end{bmatrix} e^{ik_0nd} \quad (21)$$

and dichroism

$$T_{CD} = \begin{bmatrix} \cosh\left(\frac{1}{2}k_0\Delta\kappa_{cir}d\right) & i\sinh\left(\frac{1}{2}k_0\Delta\kappa_{cir}d\right) \\ -i\sinh\left(\frac{1}{2}k_0\Delta\kappa_{cir}d\right) & \cosh\left(\frac{1}{2}k_0\Delta\kappa_{cir}d\right) \end{bmatrix} e^{-k_0\kappa d} \quad (22)$$

Here we can see that the individual operators are not diagonal (since we are using linearly polarized states as basis vectors). As a result, a complication arises because the operators do not commute. In this case it is not possible to multiply them in an arbitrary order, and yet one sequence cannot be chosen over another because birefringence and dichroism coexist. To get around this problem, Jones[26] describes an *N*-matrix formalism where one constructs for each anisotropy an operator *T** such that

$$T^*_{CB} = \left(\frac{d}{dd}T_{CB}\right){T_{CB}}^{-1} \quad (23)$$

taking circular birefrigence as an example. The next step is to construct *T** of the entire sample simply by summing the Jones *N*-matrices.

$$T^* = T^*_{CB} + T^*_{CD} \quad (24)$$

From *T** it is possible to directly obtain *T* using a method described by Jones.[26] Following this procedure we get the result

$$T = t_{iso}\begin{bmatrix} \cos\left(\frac{1}{2}k_0\Delta N_{cir}d\right) & \sin\left(\frac{1}{2}k_0\Delta N_{cir}d\right) \\ -\sin\left(\frac{1}{2}k_0\Delta N_{cir}d\right) & \cos\left(\frac{1}{2}k_0\Delta N_{cir}d\right) \end{bmatrix} e^{ik_0Nd} \quad (25)$$

where the material parameters appear in the complex refractive index $\Delta N_{cir} \equiv \Delta n_{cir} + i\Delta\kappa_{cir}$ and t_{iso} is the product of whichever Fresnel coefficients are appropriate for the substrate(s), in our case a cell bounded by two pieces of glass. The inclusion of thin-film interference for the case of circular anisotropy will be illustrated in the general case presented in section 3.3.

3.2.2. Example. As an example we consider a determination of the concentration of a solution of chiral molecules. The recorded Stokes parameters for a sucrose solution in a 5-cm cell are shown in Figure 6. That $S_3 = 0$ and that there is no variation in S_0 indicate there is no linear order, and so θ is not defined either. This suggests an isotropic distribution of chiral molecules. The angular shift in S_1 and S_2 indicates the presence of circular anisotropy, which we can attribute to the chirality of the molecules. When the above model was applied to the

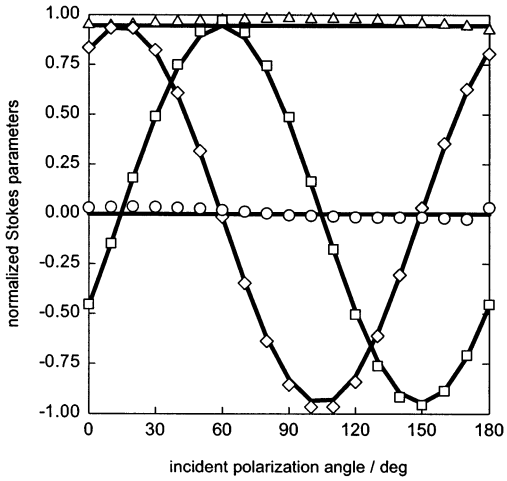

Figure 6. Sucrose solution, 0.50 g/mL, in a 5-cm cell. Stokes parameters are measured as the incident polarization angle is varied from $0 \le \psi \le \pi$ with △ S_0, ◇ S_1, □ S_2, and ○ S_3. Note the absence of linear anisotropy and circular dicroism. The primary feature is a significant angular shift in S_1 and S_2 due to circular birefringence.

data, the best fit values of the optical constants obtained were $\Delta n_{cir} = (1.024 \pm 0.052) \times 10^{-6}$ and $\Delta\alpha_{cir} = 0$. Circular dichroism is not detected because our red probe beam is very far from the absorption band of the sucrose molecules, in the UV at $\lambda = 275$ nm.[27] The concentration of the solution *c* is related to the birefringence through the specific rotation, [α].

$$c = \frac{1800°\Delta n_{cir}}{[\alpha]_{632.8}\lambda} \quad (26)$$

(For eq 26 only, it is customary to specify the wavelength λ in centimeters.) The correct [α] for our experiment is determined from

$$[\alpha]_\lambda = \frac{A}{\lambda^2 - \lambda_0^2} \quad (27)$$

where the rotation constant $A = 2.1648 \times 10^7$ deg nm^2 dm^{-1} g^{-1} mL and the dispersion constant $\lambda_0 = 146$ nm were taken from the literature.[28] Using these constants, we determine $[\alpha]_{632.8} = +57.1$ deg dm^{-1} g^{-1} mL. Substituting these values into eq 26 together with the experimentally determined Δn_{cir} gives $c = (0.51 \pm 0.02)$ g/mL. (The solution was prepared by dissolving 5.026 g of sucrose in distilled water to a total volume of 10 mL, giving a concentration of 0.50 g/mL. An Abbe refractometer was used to determine a refractive index of 1.42.)

3.3. Separation of Linear and Circular Anisotropy. *3.3.1. Description of the Polarization Change.* We now consider the most complex and interesting case of a sample that possesses all of the anisotropic optical constants. This problem may not be solved in a manner analogous to the previous cases because the eigenpolarizations are, in general, neither linear nor circular. A consequence of this is that incident light linearly polarized along the slow axis (an *e*-wave) will not be transmitted polarized along this axis, i.e., it is no longer an *e*-wave. The circular anisotropy has caused a rotation of the azimuth and a change in the ellipticity.

To begin, the incident light undergoes a basis transformation from that of the *x*- and *y*-axes of the laboratory frame to that of the slow and fast axes of the sample. The rotation $R(\theta)$ is performed in such a way that the positive *x*-axis is rotated toward the slow axis. Next, it is required to cross the air-film interface. Momentarily neglecting interference but considering the ani-

sotropy, the transmission coefficients for this interface are

$$t_{\text{slow}}^{\text{front}} = \frac{2n_{\text{air}}}{n_{\text{air}} + n_{\text{slow}}}$$

$$t_{\text{fast}}^{\text{front}} = \frac{2n_{\text{air}}}{n_{\text{air}} + n_{\text{fast}}} \tag{28}$$

which will be included in the operator for transmission across this front surface

$$t_{\text{front}} = \begin{bmatrix} t_{\text{slow}}^{\text{front}} & 0 \\ 0 & t_{\text{fast}}^{\text{front}} \end{bmatrix} \tag{29}$$

Now inside the sample, the change in field components that occurs as the wave propagates toward the back surface will be described by four Jones matrices. They are

$$T_{\text{LB}} = \begin{bmatrix} e^{-ik_0\Delta n_{\text{lin}}d/2} & 0 \\ 0 & e^{-ik_0\Delta n_{\text{lin}}d/2} \end{bmatrix} e^{ik_0nd} \tag{30}$$

and

$$T_{\text{LD}} = \begin{bmatrix} e^{k_0\Delta\kappa_{\text{lin}}d/2} & 0 \\ 0 & e^{-k_0\Delta\kappa_{\text{lin}}d/2} \end{bmatrix} e^{-k_0\kappa d} \tag{31}$$

for the linear birefringence and dichroism, respectively, and also eqs 21 and 22 for the circular birefringence and dichroism. The corresponding *N*-matrices are constructed for each of these operators, which are then added to give the *N*-matrix for the entire sample, denoted by *M**.

$$M^* = T_{\text{LB}}^* + T_{\text{LD}}^* + T_{\text{CB}}^* + T_{\text{CD}}^* \tag{32}$$

From *M** we use Jones' prescription to obtain

$$M = \begin{bmatrix} -\frac{1}{2\beta}ik_0d\Delta N_{\text{lin}}\sin\beta + \cos\beta & \frac{1}{2\beta}k_0d\Delta N_{\text{cir}}\sin\beta \\ -\frac{1}{2\beta}k_0d\Delta N_{\text{cir}}\sin\beta & \frac{1}{2\beta}ik_0d\Delta N_{\text{lin}}\sin\beta + \cos\beta \end{bmatrix} e^{ik_0Nd} \tag{33}$$

where the material parameters are contained in $\Delta N_{\text{lin}} \equiv \Delta n_{\text{lin}} + i\Delta\kappa_{\text{lin}}$, $\Delta N_{\text{cir}} \equiv \Delta n_{\text{cir}} + i\Delta\kappa_{\text{cir}}$, and $\beta \equiv \frac{1}{2}k_0d\sqrt{\Delta N_{\text{lin}}^2 + \Delta N_{\text{cir}}^2}$.

The light has now reached the back substrate, whose crossing is described by the Fresnel coefficients

$$t_{\text{slow}}^{\text{back}} = \frac{2n_{\text{slow}}}{n_{\text{slow}} + n_{\text{glass}}}$$

$$t_{\text{fast}}^{\text{back}} = \frac{2n_{\text{fast}}}{n_{\text{fast}} + n_{\text{glass}}} \tag{34}$$

which are contained in the back substrate transmission operator

$$t_{\text{back}} = \begin{bmatrix} t_{\text{slow}}^{\text{back}} & 0 \\ 0 & t_{\text{fast}}^{\text{back}} \end{bmatrix} \tag{35}$$

Finally, the light leaving the sample is expressed in terms of the laboratory frame in order to interpret the polarization change. Using these operators, the transfer function obtained from

$$T = R(-\theta)t_{\text{back}}Mt_{\text{front}}R(\theta) \tag{36}$$

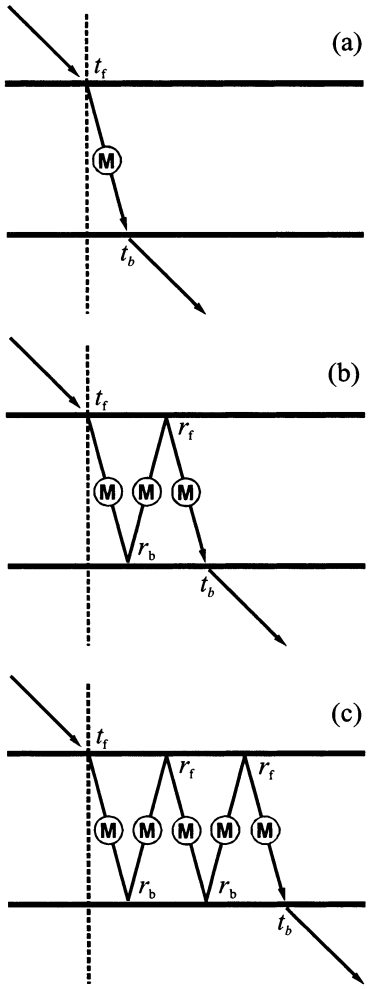

Figure 7. When the sample contains both linear and circular anisotropy, we cannot solve the interference problem by considering components of the fields along the optical axes. It is then necessary to follow the wave through the material considering transmission through the front and back interfaces (t_f and t_b), internal reflection from the front and back interfaces (r_f and r_b), and propagation inside the film (*M*). A single pass through the material is shown in (a), three passes in (b), five in (c). Finally, the output field is represented as the sum of the fields resulting from an infinite number of such passes.

describes light making a single pass through the sample, as depicted in Figure 7a.

We include the effects of interference inside the sample by considering multiple internal reflections from the two boundaries. Figure 7b would be described using the transfer function

$$T = R(-\theta)t_{\text{back}}Mr_{\text{front}}Mr_{\text{back}}Mt_{\text{front}}R(\theta) \tag{37}$$

The *r*-matrices involve the Fresnel reflection coefficients for the slow and fast axes of the sample

$$r_{\text{front}} = \begin{bmatrix} r_{\text{slow}}^{\text{front}} & 0 \\ 0 & r_{\text{fast}}^{\text{front}} \end{bmatrix} \tag{38}$$

where

$$r_{\text{slow}}^{\text{front}} = \frac{n_{\text{air}} - n_{\text{slow}}}{n_{\text{air}} + n_{\text{slow}}}$$

$$r_{\text{fast}}^{\text{front}} = \frac{n_{\text{air}} - n_{\text{fast}}}{n_{\text{air}} + n_{\text{fast}}} \tag{39}$$

and

$$r_{\text{back}} = \begin{bmatrix} r_{\text{slow}}^{\text{back}} & 0 \\ 0 & r_{\text{fast}}^{\text{back}} \end{bmatrix} \tag{40}$$

where

$$r_{\text{slow}}^{\text{back}} = \frac{n_{\text{glass}} - n_{\text{slow}}}{n_{\text{glass}} + n_{\text{slow}}}$$

$$r_{\text{fast}}^{\text{back}} = \frac{n_{\text{glass}} - n_{\text{fast}}}{n_{\text{glass}} + n_{\text{fast}}} \tag{41}$$

Figure 7c shows the light making an additional two passes through the sample before being transmitted. The actual output field is described by the sum of all the possible paths the light could take through the material. Therefore we are after

$$T = R(-\theta)t_{\text{back}}[1 + \Omega + \Omega^2 + \cdots + \Omega^{N-1}]Mt_{\text{front}}R(\theta) \tag{42}$$

where $\Omega \equiv Mr_{\text{front}}Mr_{\text{back}}$. The infinite series with Ω has a sum

$$S = \frac{1 - \Omega^N}{1 - \Omega} \tag{43}$$

Because this series is converging (all of the elements of Ω are less than unity), as $N \rightarrow \infty$, $\Omega^N \rightarrow 0$ and $S \rightarrow (1 - \Omega)^{-1}$. Finally the polarization transfer matrix for this problem, including the effects of interference, is given by

$$T = R(-\theta)t_{\text{back}}S_{\infty}Mt_{\text{front}}R(\theta) \tag{44}$$

3.3.2. Example. As an example we consider the photoinduced chirality of a liquid-crystalline azo polymer with a room-temperature nematic phase following annealing, pMAB6 [ref 29] (chemical structure shown in Figure 4b; other accounts of this polymer may be found in refs 30, 31, and 32). This material has an isotropic refractive index of 1.57 at $\lambda = 632.8$ nm, determined by observation of the Brewster angle for a probe beam with TM polarization. Photoinduced chirality has received some attention in the recent literature.[5−9] Although details of the mechanism are still in debate, it is understood that the process must involve twisting of macroscopic layers of polymer throughout the thickness of the sample, thereby creating a helical structure having optical activity governed by its handedness and pitch, among other factors.

Using the same setup as shown in Figure 1, the quarter waveplate in the Ar^+ line was rotated so that the sample was exposed to right- and/or left-circularly polarized light. A 3.88-μm sample of pMAB6 was irradiated with left-circularly polarized light for 30 min, followed by right-circularly polarized light for 30 min; results are shown in Figure 8. The fitting is a numerically intensive procedure because this parameter space is initially five-dimensional (Δn_{lin}, $\Delta\alpha_{\text{lin}}$, Δn_{cir}, $\Delta\alpha_{\text{cir}}$, θ). The convergence criterion presented in eq 20 was suitably modified to accommodate the extra two parameters for the circular anisotropy. The optical constants obtained in the data analysis are shown in Table 1. Irradiation with right-circularly polarized light resulted in dextrarotatory behavior and positive circular dichroism (Δn_{cir}, $\Delta\alpha_{\text{cir}} > 0$). Changing the handedness of the pump switched the sign of Δn_{cir} and $\Delta\alpha_{\text{cir}}$ as well. The dependence of Δn_{lin}, $\Delta\alpha_{\text{lin}}$, and θ on the handedness of the pump will be discussed in a future publication. In particular, we are currently pursuing further studies to better understand this axis of linear anisotropy, θ. For the current demonstration, it suffices to say that it is necessary and possible to separate the linear components of the anisotropy from the circular ones.

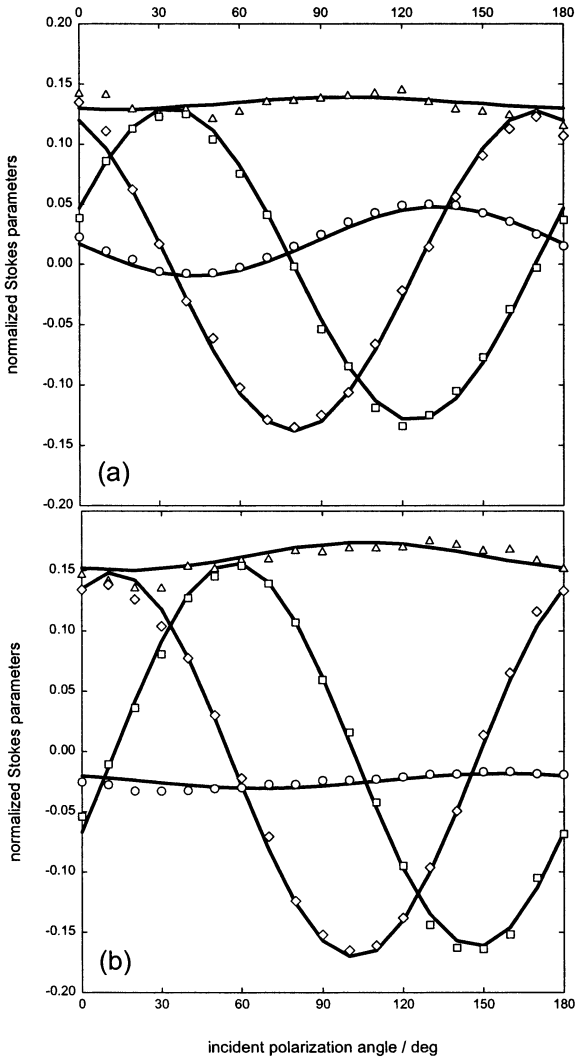

Figure 8. 8. Data obtained when pMAB6 was irradiated with (a) left-circularly polarized light and then (b) right-circularly polarized light, each for 30 min. Stokes parameters were collected as the incident polarization angle is varied from $0 \le \psi \le \pi$ with $\triangle$ S_0, $\diamond$ S_1, $\square$ S_2, and $\bigcirc$ S_3. It was observed that irradiation with left-circularly polarized light resulted in levorotatory behavior and $\Delta\alpha_{\text{cir}} < 0$; right-circularly polarized light gave dextrarotatory behavior and $\Delta\alpha_{\text{cir}} > 0$. Table 1 shows that the magnitude of the circular anisotropy is nearly the same in both cases.

TABLE 1: Anisotropic Optical Constants Determined for PMAB6 Irradiated with Circularly Polarized Light

	irradiation	
parameter	left-CP	right-CP
Δn_{lin}	$(-5.82 \pm 0.57) \times 10^{-3}$	$(-9.78 \pm 0.61) \times 10^{-4}$
Δn_{cir}	$(-9.42 \pm 0.93) \times 10^{-3}$	$(+1.08 \pm 0.07) \times 10^{-2}$
$\Delta\alpha_{\text{lin}}$ /μm^{-1}	$(-8.01 \pm 0.78) \times 10^{-3}$	$-(1.61 \pm 0.10) \times 10^{-2}$
$\Delta\alpha_{\text{cir}}$ /μm^{-1}	$(-3.33 \pm 0.33) \times 10^{-2}$	$(+3.41 \pm 0.21) \times 10^{-2}$
θ	$(+3.56 \pm 0.28)^\circ$	$(+11.5 \pm 1.1)^\circ$

4. Conclusions

When polarized light passes through materials in which the molecules are ordered, the polarization state changes as a result of interactions with these anisotropic structures. Measuring and analyzing these changes in polarization provide clues as to how

the molecules may be arranged. This allows us to develop a model for the polarization change that incorporates the anisotropic optical constants of the material. Fitting the data to the models provides the values of the constants, which serve as quantitative order parameters.

Acknowledgment. We thank the Natural Science and Engineering Research Council of Canada, and the Department of National Defence (Canada) for funding this work. D.H. thanks the Government of Ontario for an OGS scholarship. A.N., Canada Research Chair (CRC) in Polymer Chemistry, acknowledges the Government of Canada for the CRC Program.

References and Notes

(1) Natansohn, A.; Rochon, P. *Adv. Mater.* **1999**, *11*, 1387.
(2) Natansohn, A.; Rochon, P. *Can. J. Chem.* **2001**, *79*, 1093.
(3) Rochon, P.; Gosselin, J.; Natansohn, A.; Xie, S. *Appl. Phys. Lett.* **1992**, *25*, 2268.
(4) Natansohn, A.; Rochon, P.; Gosselin, J.; Xie, S. *Macromolecules* **1992**, *25*, 4.
(5) Nikolova, L.; Nedelchev, L.; Todorov, T.; Petrova, T.; Tomova, N.; Dragostinova, V.; Ramanujam, P. S.; Hvilsted, S. *Appl. Phys. Lett.* **2000**, *77*, 657.
(6) Naydenova, I.; Nikolova, L.; Ramanujam, P. S.; Hvilsted, S. *J. Opt. A: Pure Appl. Opt.* **1962**, *1*, 438.
(7) Naydenova, I.; Nikolova, L.; Todorov, T.; Andruzzi, F.; Hvilsted, S. *J. Mod. Opt.* **1997**, *44*, 1643.
(8) Ichimura, K.; Han, M. *Chem. Lett.* **2000**, *Mar.*, 286.
(9) Iftime, G.; Lagugné Labarthet, F.; Natansohn, A.; Rochon, P. *J. Am. Chem. Soc.* **2000**, *122*, 12646.
(10) Goldstein, D. H. *Appl. Opt.* **1992**, *31*, 6676.
(11) Arnaud, A.; Silveira, F.; Frins, E. M.; Dubra, A.; Perciante, C.; Ferari, J. *Appl. Opt.* **2000**, *39*, 2601.
(12) Collins, R. W.; Koh, J. *J. Opt. Soc. Am. A* **1999**, *16*, 1997.
(13) Guo, J.; Brady, D. *Appl. Opt.* **2000**, *39*, 1486.
(14) Tyo, J. S. *Opt. Lett.* **2000**, *25*, 1198.
(15) Oka, K.; Kato, T. *Opt. Lett.* **1999**, *24*, 1475.
(16) Tang, S. T.; Kwok, H. S. *J. Appl. Phys.* **2001**, *89*, 80.
(17) Rovira, P. I.; Yarussi, R. A.; Collins, R. W.; Venugopal, V. C.; Lakhtakia, A.; Messier, R.; Robbie, K.; Brett, M. J. *Thin Solid Films* **1998**, *313−314*, 373.
(18) Todorov, T.; Nikolova, L. *Opt. Lett.* **1992**, *17*, 358.
(19) A recent study (Sabatke, D. S.; Descour, M. R.; Dereniak, E. L.; Sweatt, W. C.; Kemme, S. A.; Phipps, G. S. *Opt. Lett.* **2000**, *25*, 802) has shown that optimum signal-to-noise is achieved with a retardation of 132° rather than $\lambda/4$. However, since we are rotating our compensator, the quarter waveplate is more practical.
(20) Kliger, D. S.; Lewis, J. W.; Randal, C. E. *Polarized light in optics and spectroscopy*; Academic Press: Toronto, 1990.
(21) Collett, E. *Polarized light. Fundamentals and applications*; Marcel Dekker: New York, 1993.
(22) Li, S. *J. Opt. Soc. Am. A* **2000**, *17*, 920.
(23) Azzam, R. M. A. *Opt. Lett.* **1978**, *2*, 148.
(24) Brown, D.; Natansohn, A.; Rochon, P. *Macromolecules* **1995**, *28*, 6116.
(25) Ho, M. S.; Natansohn, A.; Rochon, P. *Macromolecules* **1995**, *28*, 6124.
(26) Jones, R. C. *J. Opt. Soc. Am.* **1948**, *38*, 671.
(27) Tu, C. C. *Proc. Int. Soc. Sugar Cane Technol.* **1969**, *13*, 416.
(28) Lowry, T. M.; Richards, E. M. *J. Chem. Soc.* **1924**, *125*, 2511.
(29) Hore, D.; Natansohn, A.; Rochon, P. *J. Phys. Chem. B*, under review.
(30) Schönhals, A.; Ruhmann, R.; Carius, H.-E., Wolff, D. *Polym. Prepr.* **1997**, *38*, 429.
(31) Angeloni, A. S.; Caretti, D.; Carlini, C.; Chiellini, E.; Galli, G.; Altomare, A.; Solaro, R. *Liq. Cryst.* **1989**, *4*, 513.
(32) Hatada, K.; Kitayama, T.; Nishiura, T.; Tawada, M.; Harazona, T.; Sugaya, T. *J. Macromol. Sci.* **1997**, *A34*, 1183.